Inorg. Chem. **2008**, *47*, 1625−1633

Singlet Diradical Complexes of Ruthenium and Osmium: Geometrical and Electronic Structures and their Unexpected Changes on Oxidation

Subhas Samanta,[†] Priti Singh,[‡] Jan Fiedler,[§] Stanislav Záliš,[§] Wolfgang Kaim,*[,‡] and Sreebrata Goswami*[,†]

Department of Inorganic Chemistry, Indian Association for the Cultivation of Science, Jadavpur, Kolkata 700 032, India, Institut für Anorganische Chemie, Universität Stuttgart, Pfaffenwaldring 55, D-70550 Stuttgart, Germany, and J. Heyrovský Institute of Physical Chemistry, v.v.i., Academy of Sciences of the Czech Republic, Dolejškova 3, CZ-18223 Prague, Czech Republic

Received November 22, 2007

Reaction of HL, HL^a (2-[(2-N-phenylamino)phenylazo]pyridine), HL^b (2-[{2-N-(4-methylphenyl)amino}phenylazo]pyridine), or HL^c (2-[{2-N-(4-chlorophenyl)amino}phenylazo]pyridine), with $KRuO_4$ or OsO_4 and PPh_3 under exhaustive deoxygenation ($PPh_3 \rightarrow OPPh_3$) yields diamagnetic compounds ML_2. Crystal structure determination for $M(L^a)_2$ indicates the radical dianion state, $L^{\bullet 2-}$, for the ligands as evident from the typical N−N bond length of about 1.33 Å for a one-electron reduced azo function. The resulting spin-coupled complexes, $M^{IV}(L^{\bullet 2-})_2$, can be oxidized in two reversible one-electron steps, as probed by cyclic voltammetry and UV−vis−NIR spectroelectrochemistry. The paramagnetic intermediates, $[M(L^a)_2]^+$, are distinguished by intense NIR absorption, largely metal-centered spin as revealed by EPR, and, in the case of $[Os(L^a)_2]I_3$, by crystallographically determined shortening of the N═N bond to about 1.30 Å, corresponding to a coordinated unreduced azo function. Thus, oxidation of the complex $M^{IV}(L^{\bullet 2-})_2$ involves partial reduction of the metal in $[M^{III}(L^-)_2]^+$ because intramolecular double electron transfer is offsetting the external charge removal. Density-functional theory calculations were employed to confirm the structural features and to support the spectroscopic assignments.

Introduction

Ruthenium and osmium complexes with unsaturated nitrogen ligands have lately been among the most researched kinds of coordination compounds because the dπ(M)−π*-(ligand) interaction can effect interesting and well-accessible intramolecular charge and electron transfer processes. Energy-converting photosensitizers[1,2] of the "Ru-bpy" type ($[Ru(bpy)_3]^{2+}$) as well as mixed-valent compounds such as the Creutz-Taube ion (**1**, Scheme 1)[3] have thus found their way into standard textbooks.[4,5] Taking advantage of the kinetic stability of Ru−N and Os−N bonds and of the redox capacity of these group 8 elements, we can now describe conceptually simple ML_2 compounds, HL = 2-[(2-N-phenylamino)phenylazo]pyridines (Chart 1), with bridging transition metal centers M = Ru or Os and two electroactive peripheral conjugated tridentate ligands L^{n-}. Therefore, arrangements **2** and **3** are complementary to systems such as **1** where a π-conjugated central ligand bridges two electroactive metal sites.

Scheme 1

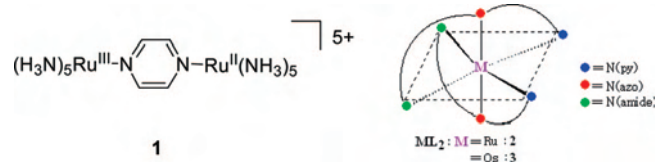

The coordination chemistry of the tridentate azoaromatic ligands (HL, Chart 1) has been investigated intensely in our

* To whom correspondence should be addressed. E-mail: icsg@iacs.res.in (S.G.), kaim@iac.uni-stuttgart.de (W.K.).
† Indian Association for the Cultivation of Science.
‡ Universität Stuttgart.
§ Academy of Sciences of the Czech Republic.

(1) (a) Grätzel, M. *Inorg. Chem.* **2005**, *44*, 6841. (b) Alstrum-Acevedo, J. H.; Brennaman, M. K.; Meyer, T. J. *Inorg. Chem.* **2005**, *44*, 6802.
(2) Wolpher, H.; Sinha, S.; Pan, J.; Johansson, A.; Lundqvist, M. J.; Persson, P.; Lomoth, R.; Bergquist, J.; Sun, L.; Sundström, V.; Åkermark, B.; Polivka, T. *Inorg. Chem.* **2007**, *46*, 638.
(3) Creutz, C. *Prog. Inorg. Chem.* **1983**, *30*, 1.
(4) Cotton, F. A.; Wilkinson, G.; Murillo, C. A.; Bochmann, M. *Advanced Inorganic Chemistry*, 6th Ed.; Wiley, New York: 1999, pp 1017–1018.
(5) (a) Shriver, D. F.; Atkins, P. W. *Inorg. Chem.*, 3rd Ed., Oxford University Press, Oxford, 1999, p 461. (b) Porterfield, W. W. *Inorganic Chemistry*; 2nd Ed., Academic Press, San Diego: 1993, pp 870–873.

10.1021/ic702301a CCC: $40.75 © 2008 American Chemical Society
Published on Web 02/05/2008

Chart 1

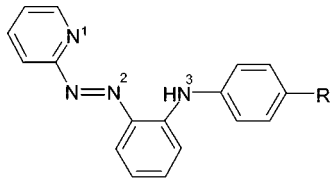

HL

R = H : HL^a
R = CH_3 : HL^b
R = Cl : HL^c

laboratory[6] during the recent years. Several novel chemical reactions and the isolation of interesting systems with unusual composition have been the focus of investigation. Our studies on these complexes have indicated that such azoaromatics can behave in a redox noninnocent way and display rich electrochemistry upon coordination. Consequently, the assignment of electronic structures of these complexes is an important issue in view of different electronic structure possibilities. We became more interested in this area after the successful isolation of a series of molybdenum complexes[7] with uncharacteristically long N−N bonds of the coordinated azo functionality. Subsequently, we have provided[8] extended evidence in favor of the existence of singlet diradical complexes of the group 6 metal elements. The topic of organic radicals coordinated to transition metal(s) is relevant to the fields of bioinorganic chemistry[9] and inorganic syntheses. Moreover, singlet diradicals are difficult to characterize because of their diamagnetic nature that may potentially cause misinterpretation[10] of the electronic structures of such systems.

In the present paper we report the synthesis and characterization of a number of ML_2 complexes (M = Ru and Os, Scheme 1). Studies of the chemical reactivity of some mixed-ligand complexes of the reference metal ions and ligands have recently been reported[11] by us. The isolation of simple bis-ligated complexes of the above type has now been achieved from high-valent metal oxo compounds, $[MO_4]^{0/-}$, in one step, using PPh_3 as reducing agent. A literature survey has revealed that such synthetic methodology involving complete oxo abstraction and subsequent ligand coordination is not commonly[7] applied. It has been possible to study the neutral parent ML_2 molecules and the mono- and dioxidized forms partially by single-crystal structure analysis (RuL_2, OsL_2, and $[OsL_2]I_3$). These studies, including EPR and UV−vis−NIR spectroelectrochemistry, have allowed us to experimentally establish oxidation states and to compare these results with density-funtional theory (DFT) calculation data.

Experimental Section

Materials. The high-valent metal oxides $K[RuO_4]$ and OsO_4 were reagents from Aldrich, and the solvents used were obtained from Qualigens and MERCK (India). The ligands HL^a−HL^c were prepared by following the reported[6] procedure. Tetrabutylammonium perchlorate (TEAP) was prepared and recrystallized as reported earlier.[12] **Caution!** *OsO_4 and perchlorate salts have to be handled with care and appropriate safety precautions.* All other chemicals were of reagent grade and were used as received.

Instrumentation. UV−vis−NIR absorption spectra were recorded on a Perkin-Elmer Lambda 950 UV/vis spectrophotometer and on a J&M TIDAS instrument. ^{1}H NMR spectra were taken on a Bruker Avance DPX 300 spectrometer, and $SiMe_4$ was used as the internal standard. Infrared spectra were obtained using a Perkin-Elmer 783 spectrophotometer. Cyclic voltammetry was carried out in 0.1 M Bu_4NClO_4 solutions using a three-electrode configuration (glassy carbon working electrode, Pt counter electrode, Ag/AgCl reference) and a PC-controlled PAR model 273A electrochemistry system. The $E_{1/2}$ for the ferrocenium−ferrocene couple under our experimental condition was 0.39 V. A Perkin-Elmer 240C elemental analyzer was used to collect microanalytical data (C, H, and N). ESI mass spectra were recorded on a micro mass Q-TOF mass spectrometer (serial No. YA 263). Spectroelectrochemistry was performed using an optically transparent thin-layer electrode (OTTLE) cell.[13a] EPR spectra in the X-band were recorded with a Bruker System EMX. A two-electrode capillary served to generate intermediates for X-band EPR studies.[13b]

Synthesis. Syntheses of the complexes were carried out by the reaction of high-valent metal oxo compounds $[MO_4]^{0/-}$ (M = Ru or Os) with the corresponding ligands in refluxing 2-methoxyethanol or methanol. The complexes of general formula ML_2 were obtained as the major products along with some unidentified minor products that are not considered here.

Synthesis of RuL_2. $Ru(L^a)_2$ **(2a):** A mixture of 120 mg (0.58 mmol) of $KRuO_4$, 320 mg (1.17 mmol) of HL^a, and 620 mg (2.5 mmol) of PPh_3 in 30 mL of 2-methoxyethanol was heated at reflux for 25 h. During this period, the color of the solution changed from red to greenish brown. The crude mass thus obtained by evaporation of the solvent was dissolved in the minimum volume of dichloromethane and was loaded on a preparative silica gel TLC plate for purification. Benzene was used as the eluent. A greenish brown zone that moved ahead of the unreacted red ligand band was collected, and the solvent was evaporated under vacuum. The residue was crystallized by slow evaporation of a dichloromethane−

(6) (a) Saha, A.; Ghosh, A. K.; Majumder, P.; Mitra, K. N.; Mondal, S.; Rajak, K. K.; Falvello, L. R.; Goswami, S. *Organometallics* **1999**, *18*, 3772. (b) Saha, A.; Majumder, P.; Goswami, S. *J. Chem. Soc., Dalton Trans.* **2000**, *11*, 1703. (c) Saha, A.; Majumder, P.; Peng, S.-M.; Goswami, S. *Eur. J. Inorg. Chem.* **2000**, *12*, 2631. (d) Kamar, K. K.; Saha, A.; Castiñeiras, A.; Hung, C.-H.; Goswami, S. *Inorg. Chem.* **2002**, *41*, 4531.

(7) Sanyal, A.; Banerjee, P.; Lee, G.-H.; Peng, S.-M.; Hung, C.-H.; Goswami, S. *Inorg. Chem.* **2004**, *43*, 7456.

(8) Sanyal, A.; Chatterjee, S.; Castiñeiras, A.; Sarkar, B.; Singh, P.; Fiedler, J.; Záliš, S.; Kaim, W.; Goswami, S. *Inorg. Chem.* **2007**, *46*, 8584.

(9) (a) Jadzewski, B. A.; Tolman, W. B. *Coord. Chem. Rev.* **2000**, *200–202*, 633. (b) Stubbe, J.; van der Donk, W. A. *Chem. Rev.* **1998**, *98*, 705. (c) Kaim, W. *Dalton Trans.* **2003**, 761.

(10) (a) Bachler, V.; Olbrich, G.; Neese, F.; Wieghardt, K. *Inorg. Chem.* **2002**, *41*, 4179. (b) Herebian, D.; Bothe, E.; Bill, E.; Weyhermüller, T.; Wieghardt, K. *J. Am. Chem. Soc.* **2001**, *123*, 10012. (c) Chaudhury, P.; Verani, C. N.; Bill, E.; Bothe, E.; Weyhermüller, T.; Wieghardt, K. *J. Am. Chem. Soc.* **2001**, *123*, 2213. (d) Bill, E.; Bothe, E.; Chaudhury, P.; Chlopek, K.; Herebian, D.; Kokatam, S.; Roy, K.; Weyhermuller, T.; Neese, F.; Wieghardt, K. *Chem.—Eur. J.* **2005**, *11*, 204.

(11) (a) Das, C.; Ghosh, A. K.; Hung, C.-H.; Lee, G.-H.; Peng, S.-M.; Goswami, S. *Inorg. Chem.* **2002**, *41*, 7125. (b) Das, C.; Peng, S.-M.; Lee, G.-H.; Goswami, S. *New J. Chem.* **2002**, *26*, 222.

(12) Goswami, S.; Mukherjee, R. N.; Chakravarty, A. *Inorg. Chem.* **1983**, *22*, 2825.

(13) (a) Krejcik, M.; Danek, M.; Hartl, F. *J. Electroanal. Chem.* **1991**, *317*, 179. (b) Kaim, W.; Ernst, S.; Kasack, V. *J. Am. Chem. Soc.* **1990**, *112*, 173.

Table 1. Crystallographic Data of **2a**, **3a**, and [**3a**]I_3

	2a	**3a**	[**3a**]I_3
empirical formula	$C_{34}H_{26}N_8Ru$	$C_{34}H_{26}N_8Os$	$C_{34}H_{26}N_8I_3Os$
molecular mass	647.70	736.83	1117.56
temperature (K)	293(2)	293(2)	293(2)
cryst syst	monoclinic	monoclinic	triclinic
space group	$P2_1/n$	$P2_1/n$	$P\bar{1}$
a (Å)	10.3999(13)	10.3341(10)	12.2467(13)
b (Å)	16.029(2)	16.0851(15)	13.1910(2)
c (Å)	16.665(2)	16.7074(16)	13.6083(15)
α (deg)	90	90	114.751(13)
β (deg)	90.256(2)	90.453(2)	103.044(9)
γ (deg)	90	90	107.607(11)
V (Å^3)	2778.0(6)	2777.1(5)	1738.1(5)
Z	4	4	2
D_{calcd} (g/cm^3)	1.549	1.762	2.135
cryst dimens (mm)	0.15 × 0.16 × 0.19	0.13 × 0.15 × 0.17	0.19 × 0.21 × 0.25
θ range for data coll (deg)	2.3−28.3	2.3−28.4	3.1−32.7
GOF	1.086	0.976	1.033
reflns collected	18325	18226	23183
unique reflns.	6872	6757	11302
largest diff. between peak and hole (eÅ^{-3})	1.36, −1.56	1.80, −1.02	2.65, −1.48
final R indices [I 2σ(I)]	R1 = 0.0578, wR2 = 0.1779	R1 = 0.0373, wR2 = 0.0817	R1 = 0.0385, wR2 = 0.1041

acetonitrile solution mixture. Yield: 60%. IR (KBr, cm^{-1}): 1591 [ν(C═N)], 1135 [ν(N═N)]. ESI-MS, *m/z*: 649 [MH]$^+$. Anal. Calcd for $C_{34}H_{26}N_8Ru$: C, 63.05; H, 4.05; N, 17.30. Found: C, 63.09; H, 4.03; N, 17.35.

Other substituted complexes (**2b** and **2c**) were similarly synthesized using the HL^b and HL^c ligands in place of HL^a. Their yields and characterization data are as follows.

Ru(L^b)$_2$ (**2b**) Yield: 55%. IR (KBr, cm^{-1}): 1591 [ν(C═N)], 1135 [ν(N═N)]. ESI-MS, *m/z*: 676 [MH]$^+$. Anal. Calcd for $C_{36}H_{30}N_8Ru$: C, 63.89; H, 4.47; N, 16.56. Found: C, 64.05; H, 4.49; N, 16.51.

Ru(L^c)$_2$ (**2c**) Yield: 53%. IR (KBr, cm^{-1}): 1583 [ν(C═N)], 1128 [ν(N═N)]. ESI-MS, *m/z*: 718 [MH]$^+$. Anal. Calcd for $C_{34}H_{24}Cl_2N_8Ru$: C, 56.98; H, 3.37; N, 15.63. Found: C, 57.03; H, 3.39; N, 15.69.

Synthesis of OsL$_2$. Os(L^a)$_2$ (**3a**): To a 40 mL methanolic solution of 2.15 g (7.87 mmol) of HL^a, 4.10 g (15.74 mmol) of PPh_3 and 1.0 g (3.93 mmol) of solid OsO_4 were added, and the mixture was refluxed for 4 h. The red solution became dark greenish brown during this period. The crude mass obtained by evaporation of the solvent was dissolved in the minimum amount of dichloromethane and was loaded on a preparative alumina TLC plate for purification. Toluene was used as eluent. A green band that moved ahead of the unreacted ligand red band was collected. Final purification of the compound was made by crystallization of a dichloromethane solution of the compound using hexane. Yield: 70%. IR (KBr, cm^{-1}): 1593 [ν(C═N)], 1135 [ν(N═N)]. ESI-MS, *m/z* 738 [MH]$^+$. Anal. Calcd for $C_{34}H_{26}N_8Os$: C, 55.42; H, 3.56; N, 15.20. Found: C, 55.45; H, 3.52; N, 15.16.

Other substituted complexes (**3b** and **3c**) were synthesized similarly using the HL^b and HL^c ligands in place of HL^a. Their yields and characterization data are as follows.

Os(L^b)$_2$ (**3b**). Yield: 60%. IR (KBr, cm^{-1}): 1600 [ν(C═N)], 1135 [ν(N═N)]. ESI-MS, *m/z*: 766 [MH]$^+$. Anal. Calcd for $C_{36}H_{30}N_8Os$: C, 56.52; H, 3.95; N, 14.65. Found: C, 56.60; H, 3.99; N, 14.56.

Os(L^c)$_2$ (**3c**). Yield: 63%. IR (KBr, cm^{-1}): 1593 [ν(C═N)], 1135 [ν(N═N)]. ESI-MS, *m/z*: 807 [MH]$^+$. Anal. Calcd for $C_{34}H_{24}N_8Cl_2Os$: C, 50.68; H, 3.00; N, 13.91. Found: C, 50.63; H, 2.98; N, 13.94.

Isolation of [M(L^a)$_2$]I$_3$. [Ru(L^a)$_2$]I$_3$. To a solution of 50 mg (0.07 mmol) of **2a** in 10 mL of dichloromethane, a solution of 25 mg (0.09 mmol) of iodine in the same solvent was added dropwise. The solution turned brown, and the solvent was evaporated in a rotary evaporator. The crude product thus obtained was thoroughly washed with hexane and was purified through crystallization by slow diffusion of a dichloromethane solution into hexane. Yield: 94% ESI-MS, *m/z*: 648 [M]$^+$. IR (KBr, cm^{-1}): 1593 [ν(C═N)], 1220 [ν(N═N)]. Anal. Calcd for $C_{34}H_{30}I_3N_8Ru$: C, 39.55; H, 2.92; N, 10.85. Found: C, 56.51; H, 2.86; N, 10.89.

Regeneration of [**2a**] from [**2a**]I_3 can be achieved by the addition of a dilute aqueous solution of N_2H_4 to an acetonitrile solution of [**2a**]I_3. The spectra and other properties of [**2a**] thus obtained match exactly with the authentic sample.

[Os(L^a)$_2$]I$_3$. Synthesis of [Os(L^a)$_2$]I_3 was made by following an identical procedure as above using **3a** in place of **2a**. Yield: 99%. ESI-MS, *m/z* 737 [M]$^+$. IR (KBr, cm^{-1}): 1593 [ν(C═N)], 1218 [ν(N═N)]. Anal. Calcd for $C_{34}H_{26}I_3N_8Os$: C, 36.54; H, 2.34; N, 10.03. Found: C, 36.50; H, 2.32; N, 9.95.

Regeneration of [**3a**] from [**3a**]I_3 was achieved following a similar procedure as described above.

Crystallography. Crystallographic data for the compounds **2a**, **3a** and [**3a**]I_3 are collected in Table 1. Suitable X-ray quality crystals of these are obtained as follows: **2a**, by slow evaporation of a dichloromethane−acetonitrile solution of the compound; **3a**, by slow diffusion of a dichloromethane solution of the compound into hexane; and [**3a**]I_3, by slow evaporation of a dichloromethane−hexane solution of the compound.

All data were collected on a Bruker SMART APEX diffractometer, equipped with graphite monochromated Mo Kα radiation (λ = 0.71073 Å), and were corrected for Lorentz-polarization effects. **2a**: A total of 18325 reflections was collected, of which 6872 were unique (R_{int} = 0.067), satisfying the ($I > 2\sigma(I)$) criterion, and were used in subsequent analysis. **3a**: A total of 18226 reflections was collected, of which 6757 were unique (R_{int} = 0.048). [**3a**]I_3**:** A total of 23183 reflections were collected, of which 11302 were unique (R_{int} = 0.039).

The structures were solved by employing the SHELXS-97 program package[14a] and were refined by full-matrix least-squares based on F^2 (SHELXL-97).[14b] All hydrogen atoms were added in calculated positions.

DFT Calculations. The electronic structure calculations on [M(L^a)$_2$] complexes and their oxidized form have been done by

(14) (a) Sheldrick, G. M. *Acta Crystallogr., Sect. A* **1990**, *46*, 467. (b) Sheldrick, G. M., *SHELXL 97. Program for the refinement of crystal structures*; University of Göttingen; Göttingen, Germany, 1997..

DFT methods using the Gaussian 03[15] program package. Spectral calculations on the neutral complexes were done by time-dependent DFT (TD-DFT).

Either the hybrid Becke's three parameter functional with the Lee, Yang, and Parr correlation functional (B3LYP)[16] or the hybrid functional of Perdew, Burke and Ernzerhof[17] (PBE0) were used together with 6–31G* polarized double-ζ basis sets[18] for C, N, and H atoms and effective core pseudopotentials and corresponding optimized sets of basis functions for Ru and Os atoms.[19] The conductor-like polarizable continuum model[20] (CPCM) was used for modeling of the solvent influence in TD-DFT calculations.

Calculations were performed without any symmetry constraints. For radical anions, a spin-unrestricted Kohn–Sham formalism was used. For analysis of singlet diradicals, a symmetry breaking approach[21,22] within DFT should be used. Therefore, the calculations on ground-state singlet states were performed using either spin-restricted or spin-unrestricted (in G03 combined with GUESS = MIX). The lowest excited states were calculated using the TD-DFT method.

Results and Discussion

Synthesis. Three ligands, HL^a−HL^c, differing with respect to substitution[6a] on the aminophenyl ring, have been used in this work is listed in Chart 1.

The ligands offer three very different kinds of N-coordination atoms, namely, a pyridyl-N (N^1), a reducible azo function containing N^2, and a diarylamido-N (N^3, after deprotonation). Pyridyl-N and azo-N are π accepting, whereas reduced azo-N and diarylamido-N are π donating.

Reactions of $KRuO_4$ (1 mmol) with the HL ligands (2 mmol) (HL^a−HL^c) in boiling 2-methoxyethanol in the presence of PPh_3 (4 mmol) produced new greenish brown RuL_2 complexes (**2a**−**c**) in 50–60% yield. Similar reactions using OsO_4 yielded the corresponding osmium complexes OsL_2 (**3a**−**c**) in 60–70% yield. The reactions of OsO_4 with HL are more facile, occurring in methanol and being complete in about 4 h. In comparison, the preparations of the ruthenium complexes need 25 h of reflux of the reaction mixtures in high-boiling 2-methoxyethanol. This is not unexpected because OsO_4 is known to be stronger oxidizing and faster reacting than $KRuO_4$.

The present synthetic strategy is based on the reduction of the metal ions via complete oxo abstraction by PPh_3 from high-valent metal oxide precursors. This methodology was developed recently by us for one-step syntheses[7] of a series of MoL_2 complexes from the reaction of ammonium heptamolybdate and HL in presence of PPh_3. It may be relevant to note here that the reactions of HL with chloride or bromide salts of the above metal ions ($RuCl_3$ or $[OsBr_6]^{2-}$) led to incomplete substitution[11] of halides, resulting in different mixed ligand halide containing metal complexes.

The complexes gave satisfactory elemental analyses (cf., Experimental Section). Electrospray mass spectra of the complexes corroborate with their formulation as ML_2 (M = Ru and Os). For example, the complex $Ru(L^a)_2$ showed an intense peak due to the molecular ion $[\mathbf{2a} + H^+]^+$ at m/z = 649 amu, and that for the osmium congener appeared at m/z = 738 amu. Notably, the experimental spectral features of the complexes correspond very well to the simulated isotopic pattern for the given formulation. A representative spectrum, that of $[\mathbf{3a} + H^+]^+$ along with the simulated spectrum, is submitted in the Supporting Information (Figure S1).

The complexes **2** and **3** possess S = 0 ground states, as determined by magnetic susceptibility measurements at room temperature. They display sharp ^{1}H NMR signals in the normal range[6] for diamagnetic compounds. The NMR spectra reveal that the ligands in ML_2 are magnetically equivalent on the NMR time scale. The ^{1}H NMR spectrum of **2a** is submitted in the Supporting Information (Figure S2).

X-ray Crystal Structures. $M(L^a)_2$ {M = Ru (2a) and M = Os (3a)}. Single-crystal X-ray structure determination (Table 1) of the two representative ruthenium and osmium complexes **2a** and **3a** revealed similar coordination and geometry and are discussed together for comparison. The ORTEP representations with atom numbering schemes of **2a** and **3a** are depicted in Figures 1 and 2, respectively. The two deprotonated tridentate ligands are coordinated by the respective metal ion using pairs of pyridyl-N, azo-N, and diarylanilido N atoms. The configuration is bis-meridional, and the relative orientations of the aforesaid pairs of coordinated atoms are cis, trans, and cis, respectively. Similar geometry and bonding was noted before[7,8] for the corresponding group 6 metal complexes $[M^{IV}L_2]$ (M = Cr, Mo, and W). Notably, the average of the chelate bite angles, $N_{pyridyl}$−M−N_{azo}, of 76.6° is systematically smaller than that of N_{azo}−M−N_{amide} (79.5°), underlining the asymmetry of the *mer*-tridentate ligands. The X-ray crystallographic analysis thus reveals considerably distorted octahedral structures with trans positioned azo-N, cis positioned 2-pyridyl-N, and cis-oriented anilido nitrogen atoms. The N_{azo}−M−N_{azo} angle is close to 170°; however, the other two trans angles are smaller at about 155° because of the overarching bite of the *mer*-tridentate ligands. Table 2 shows that DFT calculations reasonably reproduce the structures of the systems studied.

(15) Gaussian 03, Revision C.02,Frisch, M. J.; Trucks, G. W.; Schlegel, H. B.; Scuseria, G. E.; Robb, M. A.; Cheeseman, J. R.; Montgomery, J. A., Jr.; Vreven, T.; Kudin, K. N.; Burant, J. C.; Millam, J. M.; Iyengar, S. S.; Tomasi, J.; Barone, V.; Mennucci, B.; Cossi, M.; Scalmani, G.; Rega, N.; Petersson, G. A.; Nakatsuji, H.; Hada, M,; Ehara, M.; Toyota, K.; Fukuda, R.; Hasegawa, J.; Ishida, M.; Nakajima, T.; Honda, Y.; Kitao, O.; Nakai, H.; Klene, M.; Li, X.; Knox, J. E.; Hratchian, H. P.; Cross, J. B.; Bakken, V.; Adamo, C.; Jaramillo, J.; Gomperts, R.; Stratmann, R. E.; Yazyev, O.; Austin, A. J.; Cammi, R.; Pomelli, C.; Ochterski, J. W.; Ayala, P. Y.; Morokuma, K.; Voth, G. A.; Salvador, P.; Dannenberg, J. J.; Zakrzewski, V. G.; Dapprich, S.; Daniels, A. D.; Strain, M. C.; Farkas, O.; Malick, D. K.; Rabuck, A. D.; Raghavachari, K.; Foresman, J. B.; Ortiz, J. V.; Cui, Q.; Baboul, A. G.; Clifford, S.; Cioslowski, J.; Stefanov, B. B.; Liu, G.; Liashenko, A.; Piskorz, P.; Komaromi, I.; Martin, R. L.; Fox, D. J.; Keith, T.; Al-Laham, M. A.; Peng, C. Y.; Nanayakkara, A.; Challacombe, M.; Gill, P. M. W.; Johnson, B.; Chen, W.; Wong, M. W.; Gonzalez, C.; Pople, J. A. Gaussian, Inc., Wallingford, Connecticut, 2004.

(16) Becke, A. D. *J. Chem. Phys.* **1993**, *98*, 5648.

(17) Perdew, J. P.; Burke, K.; Ernzerhof, M. *Phys. Rev. Lett.* **1996**, *77*, 3865.

(18) (a) Hariharan, P. C.; Pople, J. A. *Theor. Chim. Acta* **1973**, *28*, 213. (b) Rassolov, V. A.; Pople, J. A.; Ratner, M. A.; Windus, T. L. *J. Chem. Phys.* **1998**, *109*, 1223.

(19) Andrae, D.; Häussermann, U.; Dolg, M.; Stoll, H.; Preuss, H. *Theor. Chim. Acta* **1990**, *77*, 123.

(20) Cossi, M.; Rega, N.; Scalmani, G.; Barone, V. *J. Comput. Chem.* **2003**, *24*, 669.

(21) Neese, F. *J. Phys. Chem. Solids* **2004**, *65*, 781.

(22) (a) Noodleman, L. *J. Chem. Phys.* **1981**, *74*, 5737. (b) Lahti, P. M.; Ichimura, A. S.; Sanborn, J. A. *J. Phys. Chem. A* **2001**, *105*, 251.

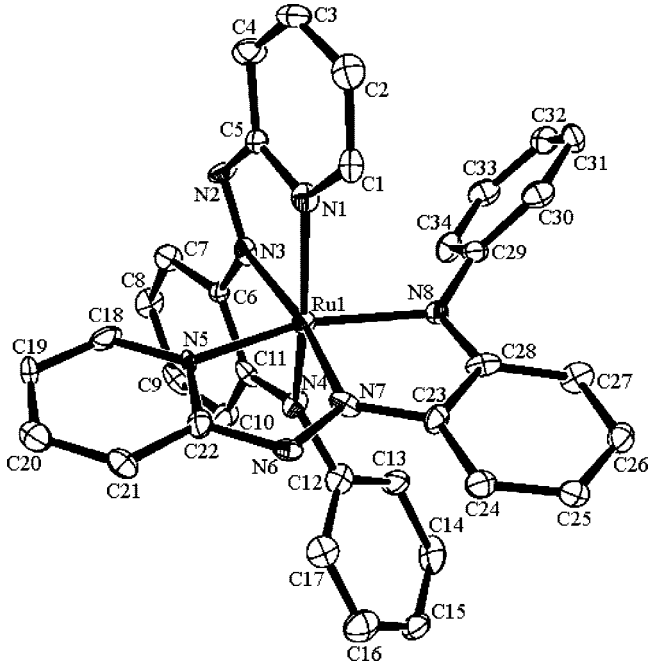

Figure 1. ORTEP representation and atom numbering scheme for $[Ru(L^a)_2]$ (**2a**).

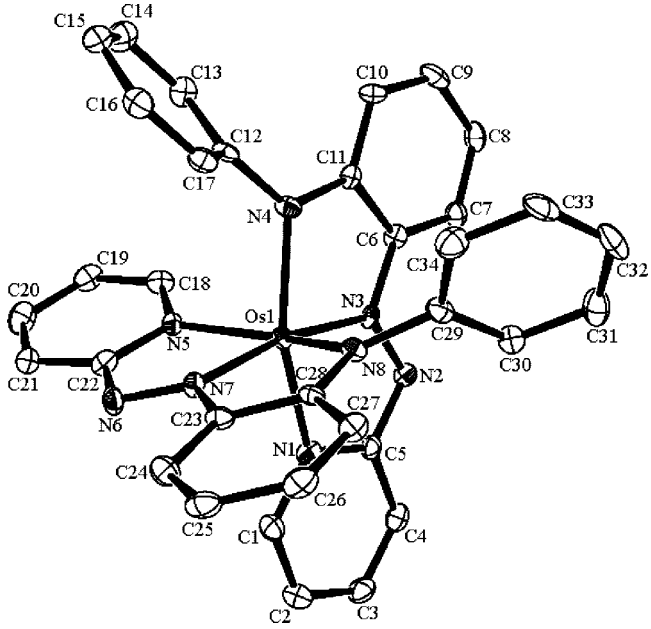

Figure 2. ORTEP representation and atom numbering scheme for $[Os(L^a)_2]$ (**3a**).

The N−N distance is an excellent indicator of the charge on an azo function.[23] From the ca. 1.24 Å for free ligands, the coordination by back-donating metals may shift this value to about 1.25–1.30 Å. Real one-electron reduced (i.e., anion radical) ligands as calculated (Re^I, $Ru^{2.5}$)[24] and structurally characterized (Ru^{II}, Os^{II})[25] and as independently verified through EPR based spin distribution analysis (Cu^I complexes)[26] have about 1.35 Å, whereas the two-electron reduced hydrazido(2−) ligands have single bonds[23,27] with d(N−N) > 1.40 Å. Similar structure/oxidation state correlations are known for the complexes of the O_2^{n-} ligands[28] and for *o*-quinone-type (1,2-dioxolene) ligands.[29]

In the present case, the nonoxidized ML_2 molecules have d(N−N) ≈ 1.33 Å (Table 2), clearly suggesting the radical dianion form of the ligand (one charge from deprotonation at N^3 and another from one-electron reduction centered on the azo function), and, by implication, the +IV state for the metals, M = Ru or Os,: $M^{IV}(L^{\bullet 2-})_2$. The same conclusion as derived here for M = Ru and Os was obtained[8] for M = Cr, Mo, and W with d(N−N) ranging from 1.339(2) to 1.373(3) Å. All of these diamagnetic molecules may thus be viewed as singlet diradical[10,30,31] species, a description that has recently been propagated, e.g., for bis(semiquinone) and ruthenium trithiolate complexes. In the present situation the electrons from a d^4 configuration at the metals couple with the singly occupied ligand molecular orbitals (MOs) to create a spin-paired entity, as is confirmed by the DFT calculations (cf. below).

The metal−nitrogen bonds in these complexes are unexceptional, lying in the range 1.95−2.07 Å. The effects of −N=N− bond elongation of the coordinated ligands in the present complexes are reflected by the lowering of vibrational frequencies $\nu_{N=N}$ as compared to uncoordinated HL. The $\nu_{N=N}$ band in free HL appears around 1380 cm^{-1}, whereas those in the present complexes are considerably lower,[32] appearing near 1135 cm^{-1}.

The one-electron oxidized form of the osmium complex could be crystallized as triiodide, allowing us to establish the N−N bond lengths in the ligands (cf. below) at close to 1.30 Å (average, cf. Table 2). The ORTEP representation with atom numbering scheme of the compound is displayed in Figure 3. The coordination geometry of the oxidized complex is similar to that of the parent complex, [**3a**]. However, the most striking feature of this structure is the notable contraction of the N−N bond length. Accordingly

(23) Kaim, W. *Coord. Chem. Rev.* **2001**, *219–221*, 463.
(24) (a) Frantz, S.; Hartmann, H.; Doslik, N.; Wanner, M.; Kaim, W.; Kümmerer, H. J.; Denninger, G.; Barra, A.-L.; Duboc-Toia, C.; Fiedler, J.; Ciofini, I.; Urban, C.; Kaupp, M. *J. Am. Chem. Soc.* **2002**, *124*, 10563. (b) Sarkar, B.; Patra, S.; Fiedler, J.; Sunoj, R. B.; Janardanan, D.; Mobin, S. M.; Niemeyer, M.; Lahiri, G. K.; Kaim, W. *Angew. Chem., Int. Ed.* **2005**, *44*, 5655.
(25) (a) Shivakumar, M.; Pramanik, K.; Ghosh, P.; Chakravorty, A. *J. Chem. Soc. Chem. Commun.* **1998**, *19*, 2103. (b) Shivakumar, M.; Pramanik, K.; Ghosh, P.; Chakravorty, A. *Inorg. Chem.* **1998**, *37*, 5968. (c) Pramanik, K.; Shivakumar, M.; Ghosh, P.; Chakravorty, A. *Inorg. Chem.* **2000**, *39*, 195.
(26) (a) Doslik, N.; Sixt, T.; Kaim, W. *Angew. Chem., Int. Ed.* **1998**, *37*, 2403. (b) Kaim, W.; Doslik, N.; Frantz, S.; Sixt, T.; Wanner, M.; Baumann, F.; Denninger, G.; Kümmerer, H.-J.; Duboc-Toia, C.; Fiedler, J.; Záliš, S. *J. Mol. Struct.* **2003**, *656*, 183.
(27) (a) Chan, D.; Cronin, L.; Duckett, S. B.; Hupfield, P.; Perutz, R. N. *New J. Chem.* **1998**, *22*, 511. (b) Morino, Y.; Iijima, T.; Murata, Y. *Bull. Chem. Soc. Jpn.* **1960**, *33*, 46. (c) Marabella, C. P.; Enemark, J. H.; Newton, W. E.; McDonald, J. W. *Inorg. Chem.* **1982**, *21*, 623. (d) Ittel, S. D.; Ibers, J. A. *Inorg. Chem.* **1973**, *12*, 2290. (e) Muñiz, K.; Nieger, M. *Angew. Chem., Int. Ed.* **2006**, *45*, 2305.
(28) Cotton, F. A.; Wilkinson, G.; Murillo, C. A.; Bochmann, M. *Advanced Inorganic Chemistry*, 6th ed., Wiley, New York, 1999, pp. 468–471.
(29) Bhattacharya, S.; Gupta, P.; Basuli, F.; Pierpont, G. C. *Inorg. Chem.* **2002**, *41*, 5810.
(30) Herebian, D.; Wieghardt, K. E.; Neese, F. *J. Am. Chem. Soc.* **2003**, *125*, 10997.
(31) Grapperhaus, C. A.; Kozlowski, P. M.; Kumar, D.; Frye, H. N.; Venna, K. B.; Poturovic, S. *Angew. Chem., Int. Ed.* **2007**, *46*, 4085.
(32) Itoh, T.; McCreery, R. L. *J. Am. Chem. Soc.* **2002**, *124*, 10894.

Table 2. Selected Experimental Bond Lengths (Å) and trans Angles (°) of $[M(L^a)_2]^{0/+}$ Complexes

	(**2a**)		(**3a**)		[**3a**]I_3	
bond	Exp.	Calc.	Exp.	Calc.	Exp.	Calc.
M−N1	2.075(5)	2.067	2.047(3)	2.064	2.062(4)	2.081
M−N3	1.966(5)	1.968	1.967(3)	1.976	1.973(5)	1.988
M−N4	2.056(5)	2.095	2.074(3)	2.097	1.999(4)	2.038
M−N5	2.041(4)	2.067	2.058(3)	2.063	2.077(5)	2.088
M−N7	1.960(4)	1.968	1.955(3)	1.976	1.973(5)	1.996
M−N8	2.079(5)	2.095	2.036(3)	2.097	1.995(4)	2.026
N2−N3	1.324(7)	1.307	1.334(4)	1.312	1.303(7)	1.299
N6−N7	1.327(6)	1.307	1.341(5)	1.313	1.310(7)	1.295
N3−C6	1.378(7)	1.367	1.393(6)	1.381	1.394(7)	1.376
N7−C23	1.375(7)	1.368	1.382(6)	1.381	1.398(7)	1.378
N4−C11	1.357(8)	1.343	1.370(5)	1.356	1.378(8)	1.413
N8−C28	1.320(7)	1.342	1.358(5)	1.355	1.386(8)	1.414
N3−M−N7	170.21(19)	172.5	168.76(13)	167.3	175.80(19)	176.2
N1−M−N4	154.47(17)	155.5	154.48(12)	152.8	153.77(18)	154.6
N5−M−N8	155.70(18)	155.6	152.08(12)	152.7	154.2(2)	155.1

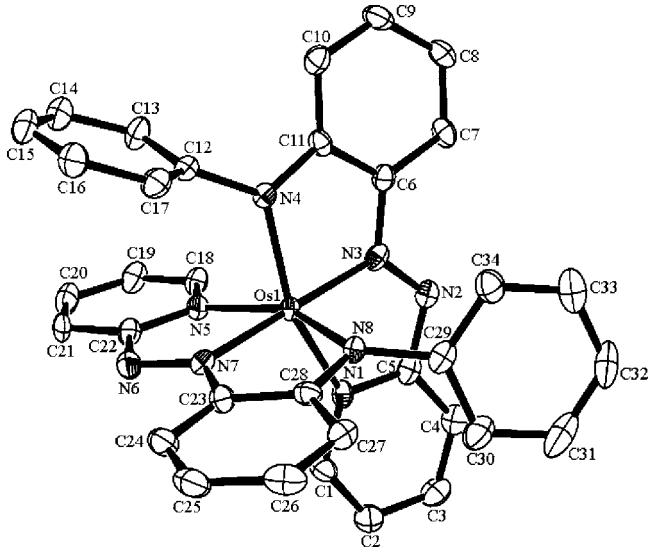

Figure 3. ORTEP representation and atom numbering scheme for $[Os(L^a)_2]^+$ (**3a**$^+$) in [**3a**]I_3

Table 3. Cyclic Voltammetry Data[a] of $[ML_2]$ **2a**−**c** and **3a**−**c**

compound	oxidation $E_{1/2}$,[b] V (ΔE_p, mV)	reduction $-E_{1/2}$,[b] V (ΔE_p, mV)
$[Ru(L^a)_2]$ (**2a**)	0.04 (70), 0.76 (80)	1.15 (70)
$[Ru(L^b)_2]$ (**2b**)	0.01 (70), 0.73 (75)	1.13(70)
$[Ru(L^c)_2]$ (**2c**)	0.11 (80), 0.78 (80)	1.06 (65)
$[Os(L^a)_2]$ (**3a**)	−0.03 (75), 0.62(80)	1.13 (75)
$[Os(L^b)_2]$ (**3b**)	−0.06 (70), 0.58 (75)	1.08 (70)
$[Os(L^c)_2]$ (**3c**)	−0.01 (75), 0.64 (80)	1.11 (75)

[a] In dichloromethane solution, supporting electrolyte Bu_4NClO_4 (0.1 M), reference electrode SCE. [b] $E_{1/2} = 0.5(E_{pa} + E_{pc})$ where E_{pa} and E_{pc} are anodic and cathodic peak potentials, respectively; $\Delta E_p = E_{pa} - E_{pc}$; scan rate = 50 mV s^{-1}.

the $\nu_{N=N}$ band in [**2a**]I_3 and [**3a**]I_3 appears at a higher frequency (near 1220 cm^{-1}) than that (1135 cm^{-1}) in the corresponding reduced complex.

This corresponds to monoanionic ligands with unreduced azo functions coordinated to a transition metal,[6,23,33] and as a consequence, one may surmise the formulation $[M^{III}(L^-)_2]^+$. The alternative resonance forms $[(L^-)M^{IV}(L^{\bullet 2-})]^+ \leftrightarrow [(L^{\bullet 2-})M^{IV}(L^-)]^+$ would have to assume valence delocalization between one radical dianion and one monoanion ligand that are perpendicularly oriented; such a description is considered to be less plausible, as will also be discussed below in connection with EPR (metal-centered spin) and UV−vis−NIR results (NIR absorption).The compounds [**2a**]I_3 and [**3a**]I_3 both are 1:1 electrolytes in acetonitrile. Their elemental analyses as well as ESI-mass spectra are consistent with their formulations. The magnetic moments at 298 K of the solid samples of [**2a**]I_3 and [**3a**]I_3 are 1.68 and 1.55 μ_B, respectively, signifying the presence of one unpaired electron.

The fact that oxidation of the complex would cause a reduction of the metal seems paradoxical but has been similarly observed in quinone and TCNX chemistry; the combined oxidation state change of more than one component (ligand or metal) is capable of offsetting a counterintuitive electron transfer of the single center (metal or ligand). Thus, the reduction of tris(*o*-semiquinonato)vanadium(III) produced[34] a tris(catecholato)vanadium(V) anion, and the reduction of $\{(\mu_4\text{-}TCNE^{2-})[Ru^{2.5}(NH_3)_5]_4\}^{8+}$ gives[35] $(\mu_4\text{-}TCNE^{\bullet -})[Ru^{II}(NH_3)_5]_4\}^{7+}$.

The Electronic Structures of $[M(L^a)_2]^{0,+}$ (M = Ru and Os). All neutral complexes examined are diamagnetic species; therefore, the geometry optimizations were performed for singlet ground states. Calculations were done using both the restricted and the unrestricted approach. The structures of all systems are better described by using the PBE0 hybrid functional than by using B3LYP; the results depend only slightly on the approach used. Calculated selected bond lengths and angles are compared with experimental ones in Table 2. The calculated structural parameters within both neutral complexes are in very good agreement with the experimental structure; the variation of intraligand bond lengths due to the central atom and the charge variations are also well described by the calculations. A previously published[8] geometry optimization of the uncoordinated protonated (2-phenyl)-substituted ligand radical anion gave N−N, N2−C12, and N1−C7 bond lengths of 1.317, 1.365, and 1.397 Å, respectively. These values are quite close to

(33) Hartmann, H.; Scheiring, T.; Fiedler, J.; Kaim, W. *J. Organomet. Chem.* **2000**, *604*, 267.

(34) (a) Pierpont, C. G.; Lange, C. W. *Prog. Inorg. Chem.* **1994**, *41*, 331. (b) Cass, M. E.; Gordon, N. R.; Pierpont, C. G. *Inorg. Chem.* **1986**, *25*, 3962.

(35) (a) Moscherosch, M.; Waldhör, E.; Binder, H.; Kaim, W.; Fiedler, J. *Inorg. Chem.* **1995**, *34*, 4326. (b) Waldhör, E.; Kaim, W.; Lawson, M.; Jordanov, J. *Inorg. Chem.* **1997**, *36*, 3248.

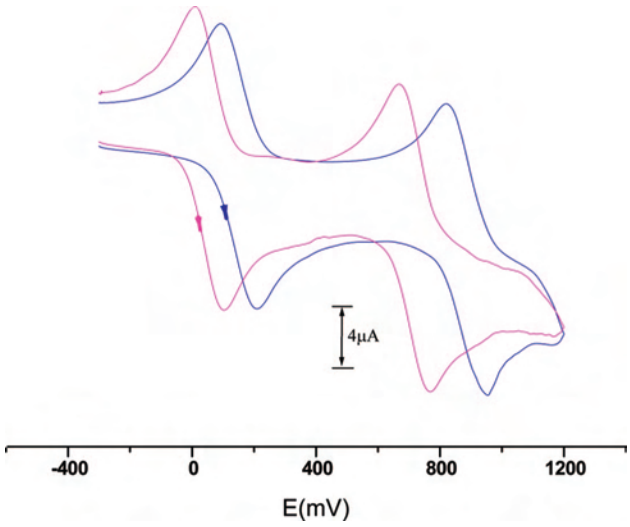

Figure 4. Cyclic voltammograms of the complexes $Ru(L^a)_2$ (blue) and $Os(L^a)_2$ (pink) in CH_2Cl_2/0.1 M Bu_4NClO_4.

Table 4. EPR Data[a] of Monocation Intermediates $[M(L^a)_2]^+$

	M = Ru	M = Os
g_1	2.148	2.386
g_2	2.113	2.283
g_3	1.965	1.848
g_{av}[b]	2.077	2.185
$g_{av} - g_e$[c]	0.075	0.183
$\Delta g = g_1 - g_3$	0.183	0.538
ξ (cm^{-1})[d]	1200	3000

[a] From oxidation in CH_2Cl_2/0.1 M Bu_4NPF_6, recording at 4 K. [b] Isotropic values at 295 K: 2.076 ($[Ru(L^a)_2]^+$), 2.180 $[Os(L^a)_2]^+$). [c] $g_e = 2.0023$ (free electron value). [d] Spin–orbit coupling constants for M^{3+} (from ref 36).

the ones calculated for the neutral $[M(L)_2]$ complexes, which indicates the radical anion ligand character of the bound ligands. The elongation of the N−N bond length due to the reduction of the ligand is comparable with the elongation caused by metal coordination. The DFT calculated charges on the central metal atoms are 1.07 and 1.35 for the Ru and Os systems, respectively. In agreement with the experiment, the DFT calculations as listed in Table 2 predict a contraction of the N−N bonds following the oxidation of $[Os(L^a)_2]$ together with other structure variations: elongation of M−N1 and M−N5 distances and a remarkable shortening of the M−N4 and M−N8 bond lengths.

The energies and compositions of the DFT calculated frontier orbitals are similar for both $[RuL_2]$ and $[OsL_2]$ complexes; they are listed in the Supporting Information (Tables S1 and S2). The MO representations show the highest occupied MO (HOMO) to be formed by a combination of d metal orbitals (27% and 25% for Ru and Os complexes, respectively) and π ligand orbitals. Closely lying occupied HOMO-1 is formed by π ligand orbitals, and the next three lower lying occupied orbitals have larger contributions (over 46%) from the corresponding central metal atom. The almost degenerate set of lowest lying unoccupied MOs (LUMOs) is, to a large extent, delocalized over the π system of the ligands; d orbitals contribute to this orbital only by 14–21%. The higher unoccupied MOs also have ligand character.

Electrochemistry. Cyclic voltammetry of RuL_2 (**2a**−**c**) complexes in CH_2Cl_2 exhibits two reversible oxidation waves and one irreversible cathodic process (Table 3 and Figure 4). One-electron stoichiometry of the reversible processes is confirmed by exhaustive electrolyses of the representative compound **2a** at 0.25 and 1.00 V, respectively. The redox potentials are found to be sensitive to the nature of substitution on the amino phenyl ring. Thus, a gradual shift of the reduction potential to more positive values is observed upon moving from **2b** (0.01 and 0.73 V) via **2a** (0.04 and 0.76 V) to **2c** (0.11 and 0.78 V). The first oxidation potential is low, and accordingly, we have succeeded in isolating a representative cationic complex [**2a**]I_3 in the pure state, using iodine as the oxidizing agent. The osmium analogue is more crystalline (vide supra), and its X-ray structure has been solved. Notably, the reduced complexes [**2a**] and [**3a**] can be regenerated quantitatively from [**2a**]I_3 and [**3a**]I_3, respectively, by the use of hydrazine as reducing agent. Our attempts to isolate the dicationic complex $[\mathbf{2a}]^{2+}$ have so far been unsuccessful. However, characterization of both $[\mathbf{2a}]^+$ and $[\mathbf{2a}]^{2+}$ was achieved by spectroelectrochemical measurements (cf. below).

The osmium analogues OsL_2 (**3a**−**c**) show similar redox behavior (Table 3). Examination of the data in Table 3 indicates that the osmium complexes are oxidized more easily than the ruthenium congeners by 100−150 mV, an expected

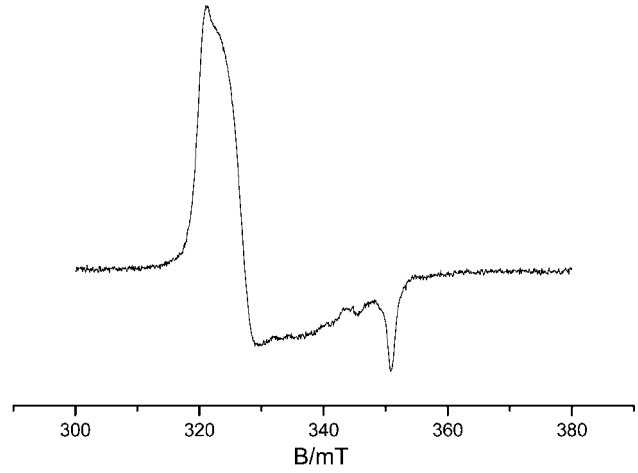

Figure 5. EPR Spectrum of electrogenerated $[Ru(L^a)_2]^+$ ($\mathbf{2a}^+$) in CH_2Cl_2/0.1 M Bu_4NPF_6 at 4K.

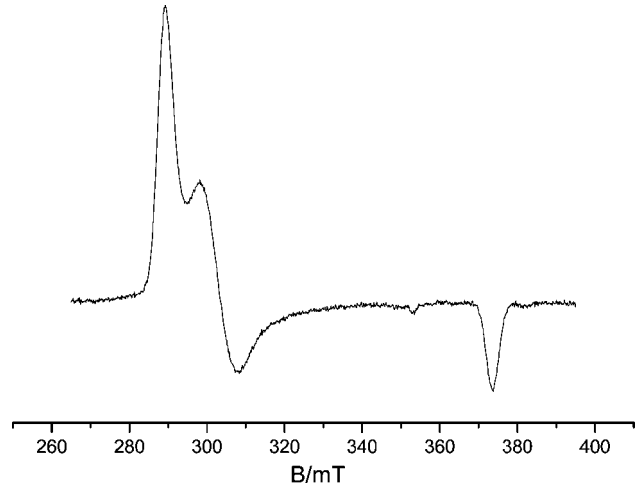

Figure 6. EPR Spectrum of electrogenerated $[Os(L^a)_2]^+$ ($\mathbf{3a}^+$) in CH_2Cl_2/0.1 M Bu_4NPF_6 at 4K.

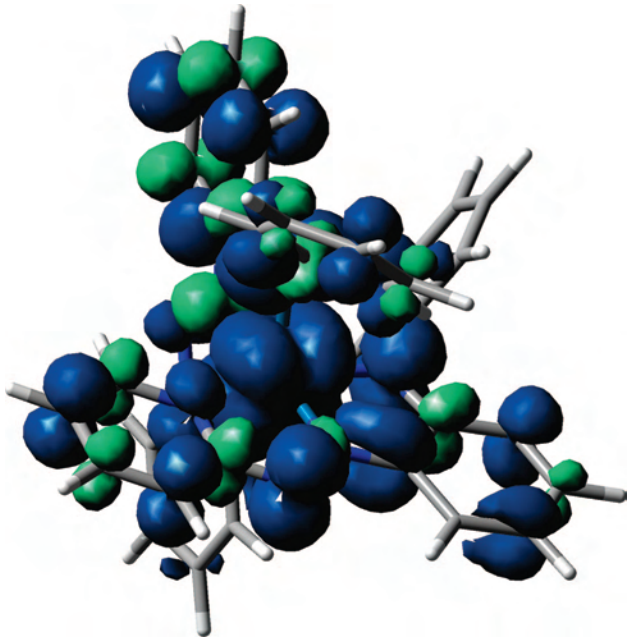

Figure 7. DFT calculated spin densities for $[Os(L^a)_2]^+$. The blue and green areas correspond to regions of positive and negative spin density, respectively.

result. Chemical oxidation of **3a** by iodine followed by crystallization thus produced X-ray quality crystals of [**3a**]I_3.

EPR Spectroscopy. The two monocations $\mathbf{2a}^+$ and $\mathbf{3a}^+$ show a similar splitting pattern of the *g* components in frozen solution (Table 4, Figures 5 and 6). Two close lying components $g_1, g_2 > 2$ are complemented by $g_3 < 2$. Taken together with $g_{av} > 2$, this is typical for a low-spin d^5 situation (Ru^{III} and Os^{III}) with not-too-distorted octahedral ligation. Clearly, the deviation of *g* factor components and of the average *g* (g_{av}) from *g*(electron) [g_e] = 2.0023 is larger for the osmium alternative because of the much higher spin–orbit coupling constant ξ of the 5d element;[36] remarkably, both the total *g* anisotropy $\Delta g = g_1 - g_3$ and the deviation $g_{av} - g_e$ are about 2.5 times as large for the Os system, in accordance with the similar ratio between $\xi(Os^{3+}) = 3000\ cm^{-1}$ and $\xi(Ru^{3+}) = 1200\ cm^{-1}$.[36]

In absolute terms, the values from Table 4 are intermediate between those of M^{II} containing radicals and of true M^{III} systems, that is, those without significant metal–ligand orbital mixing.[37] The data for the ruthenium derivative correspond to values that have been reported for complexes $[(Q)Ru(acac)_2]^n$, Q = *o*-imino(thio)quinone, $n = -$ or $+$, and which have been thoroughly analyzed in a theoretical study.[38] Drawing similar conclusions, we assume largely metal-centered spin corresponding to M^{III} systems, $[M^{III}(L^-)_2]^+$, with, however, very significant participation of the potentially noninnocent ligands $L^{-/\bullet 2-}$. These conclusions are qualitatively supported by DFT (PBE0) calculations of $[Os(L^a)_2]^+$, which gives a spin density of 0.530 for Os; the remaining spin density is distributed over the ligand system (Figure 7).

(36) Weil, J. A.; Bolton, J. R. *Electron Paramagnetic Resonance*, 2nd Ed., Wiley Interscience, New York, 2007.
(37) Patra, S.; Sarkar, B.; Mobin, S. M.; Kaim, W.; Lahiri, G. K. *Inorg. Chem.* **2003**, *42*, 6469.

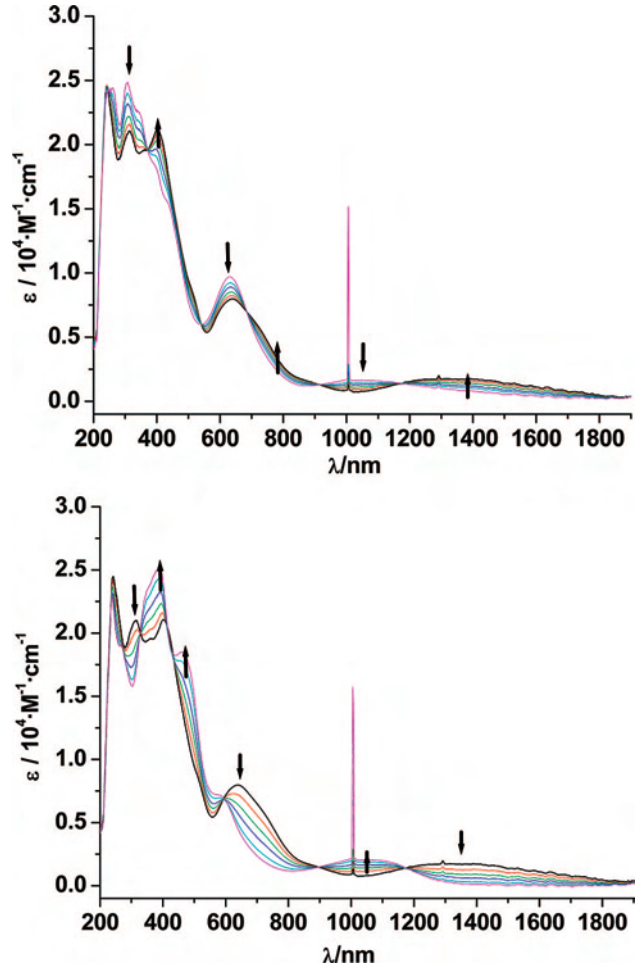

Figure 8. UV−vis−NIR Spectroelectrochemical response of $Os(L^a)_2$ (**3a**) in CH_2Cl_2/0.1 M Bu_4NPF_6 during the first (top) and the second oxidation (bottom).

UV−vis−NIR Spectroelectrochemistry. The absorption spectral changes upon stepwise reversible one-electron oxidation of ML_2 complexes are shown in Figure 8 for the osmium compound with L^a, the data are summarized in Table 5.

Neutral and dicationic forms exhibit rather similar low-energy absorption spectra with a weaker band around 1200 (Ru) or 1000 nm (Os) and another one at 660/530 (Ru) or 600 nm (Os). The EPR active intermediates show long-wavelength shifted absorptions at about 1800 and 800/700 nm (Ru) or 1320 and 640 nm (Os). The assignment of these bands is based on structural and EPR information for the oxidation state distribution in the ground-state and on the results of TD-DFT calculations. As shown in Table 5, the TD-DFT calculations qualitatively describe the main features of the absorption spectra for the neutral Ru and Os complexes quite well. The band around 1000 nm is assigned to involve HOMO → LUMO and HOMO → LUMO + 1 excitations with a predicted shift of this band to longer wavelengths when going from Os to Ru. The next features within the spectra around 600 nm can be assigned to HOMO − 1 → LUMO and HOMO − 1 → LUMO + 1 excitations. The intense broad band at shorter wavelength is composed

(38) Remenyi, C.; Kaupp, M. *J. Am. Chem. Soc.* **2005**, *127*, 11399.

Table 5. Absorption Maxima for $[ML_2]^{n+}$ from UV−vis−NIR Spectroelectrochemistry and TD-DFT Calculated Lowest-Lying Transitions for $[M(L^a)_2]$ complexes[a]

complex	λ_{max}/nm (ϵ/M^{-1} cm^{-1})
$[Ru(L^a)_2]$	1150 (1575), 675 (8500), 555 (7730), 450 (15 770), 410 (13 330), 315 (22 965), 245 (26 220)
$[Ru(L^a)_2]^b$	1074 (0.015), 1025 (0.024), 652 (0.091), 630 (0.138), 480 (0.105), 449 (0.040), 416 (0.073), 395 (0.199), 372 (0.126), 361 (0.206), 358 (0.128), 349 (0.098), 309 (0.073)
$[Ru(L^b)_2]$	1155 (1410), 680 (7290), 556 (6610), 452 (13 080), 413 (11 680), 313 (20 270), 230 (27 445)
$[Ru(L^c)_2]$	1155 (1055), 678 (5380), 550 (5395), 445 (10 830), 405sh, 315sh, 280sh, 250 (31 145)
$[Ru(L^a)_2]^+$	1800 (1490), 790sh, 708 (7160), 496sh, 420sh, 355sh, 299sh
$[Ru(L^a)_2]^{2+}$	1290 (2700), 1125sh, 649sh, 510sh, 456 (12 510), 367 (24 120)
$[Os(L^a)_2]$	1003 (1280), 630 (9680), 435sh, 395sh, 345sh, 305 (24 790), 260 (24 470)
$[Os(L^a)_2]^b$	978 (0.026), 635 (0.076), 604 (0.120), 428 (0.093), 389 (0.208), 363 (0.130), 359 (0.138), 352 (0.136), 351 (0.136), 351 (0.186), 349 (0.142)
$Os(L^b)_2]$	1050 (1020), 630 (8640), 430sh, 400sh, 310sh, 255 (29 125)
$[Os(L^c)_2]$	1055 (960), 635 (7520), 435sh, 395sh, 310sh, 250 (27 430)
$[Os(L^a)_2]^+$	1320 (1750), 710sh, 639 (7970), 401 (21 180), 360sh, 313(21 080)
$[Os(L^a)_2]^{2+}$	1003 (2170), 590sh, 462 (18 520), 388 (25 140)

[a] In CH_2Cl_2/0.1 M Bu_4NPF_6. [b] TD DFT-calculated transitions, oscillator strengths in parenthesis. Only transitions with oscillator strength larger than 0.01 are presented.

Scheme 2

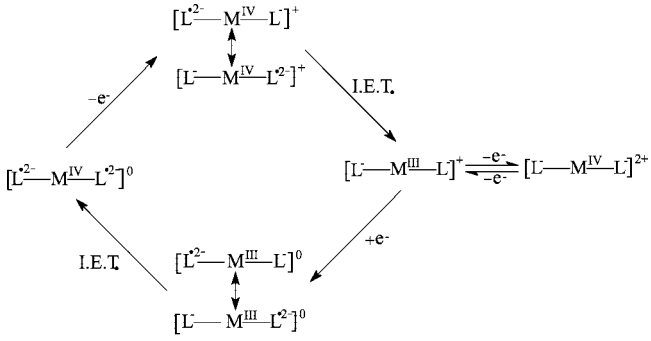

I.E.T. = Internal Electron Transfer

of many intense transitions, most of which have some metal-to-ligand charge transfer (MLCT) character.

The $L^{\bullet 2-}/M^{IV}/L^{\bullet 2-}$ singlet diradical ground-state can be converted to excited states approximately described as $*[L^-/M^{III}/L^{\bullet 2-}]$ in ligand-to-metal charge transfer (LMCT) processes. The monocations, on the other hand, identified by EPR and structure analysis as $[L^-/M^{III}/L^-]^+$ species, may be excited to $*[L^-/M^{IV}/L^{\bullet 2-}]^+$ in MLCT transitions. MLCT transitions are also believed to cause the low-energy absorption bands in $[L^-/M^{IV}/L^-]^{2+}$, leading to $*[L^-/M^{V}/L^{\bullet 2-}]^{2+}$ or $*[L^{\bullet 2-}/M^{VI}/L^{\bullet 2-}]^{2+}$. Such excited states correspond to the ground states of the ML_2 complexes, M = Mo^{IV} or W^{IV}, described earlier.[8]

Conclusion

Employing high-valent oxo-ruthenium or -osmium precursors and PPh_3 as reducing agent in the presence of tridentate azo-containing ligands, we have synthesized new singlet diradical complexes of Ru^{IV} or Os^{IV} with the corresponding dianion radical species. Experimental (X-ray diffraction) and theoretical studies (DFT) support this interpretation that could be extended to the oxidized states formed via two one-electron steps (Scheme 2). Structural effects (N−N bond shortening), EPR results (metal-centered spin), and spectroelectrochemical information in conjunction with DFT calculations confirm the oxidation of both ligands but reduction of the metal in the first oxidation process.

Acknowledgment. Financial support from the Department of Science and Technology (DST)(Project SR/S1/IC-24/2006) and the Council of Scientific and Industrial Research, New Delhi, from the Deutsche Forschungsgemeinschaft and Fonds der Chemischen Industrie (Frankfurt/Main), and from the Grant Agency of the Czech Republic (KAN100400702) and the Ministry of Education of the Czech Republic (COST Grants OC 139 and OC 140) is gratefully acknowledged. Crystallography was performed at the DST-funded National Single Crystal Diffractometer Facility at the Department of Inorganic Chemistry, IACS. S. S. also thanks the Council of Scientific and Industrial Research for his fellowship.

Supporting Information Available: X-ray crystallographic files in CIF format for **2a**, **3a**, and [**3a**]I_3; figures of ESI-MS for **3a** (S1); ^{1}H NMR of **2a** (S2); and cyclic voltammograms of **2a** and **3a** in CH_2Cl_2/ 0.1 M Bu_4NClO_4 (S3) are provided. This material is available free of charge via the Internet at http://pubs.acs.org.

IC702301A